CLNS 07/1998
CLEO 07-07

Measurement of the total hadronic cross section in e^+e^- annihilation below 10.56 GeV

D. Besson,[1] T. K. Pedlar,[2] D. Cronin-Hennessy,[3] K. Y. Gao,[3] J. Hietala,[3] T. Klein,[3] Y. Kubota,[3] B. W. Lang,[3] R. Poling,[3] A. W. Scott,[3] A. Smith,[3] P. Zweber,[3] S. Dobbs,[4] Z. Metreveli,[4] K. K. Seth,[4] A. Tomaradze,[4] J. Ernst,[5] K. M. Ecklund,[6] H. Severini,[7] S. A. Dytman,[8] W. Love,[8] V. Savinov,[8] O. Aquines,[9] A. Lopez,[9] S. Mehrabyan,[9] H. Mendez,[9] J. Ramirez,[9] G. S. Huang,[10] D. H. Miller,[10] V. Pavlunin,[10] B. Sanghi,[10] I. P. J. Shipsey,[10] B. Xin,[10] G. S. Adams,[11] M. Anderson,[11] J. P. Cummings,[11] I. Danko,[11] D. Hu,[11] B. Moziak,[11] J. Napolitano,[11] Q. He,[12] J. Insler,[12] H. Muramatsu,[12] C. S. Park,[12] E. H. Thorndike,[12] F. Yang,[12] M. Artuso,[13] S. Blusk,[13] J. Butt,[13] J. Li,[13] N. Menaa,[13] R. Mountain,[13] S. Nisar,[13] K. Randrianarivony,[13] R. Sia,[13] T. Skwarnicki,[13] S. Stone,[13] J. C. Wang,[13] K. Zhang,[13] G. Bonvicini,[14] D. Cinabro,[14] M. Dubrovin,[14] A. Lincoln,[14] D. M. Asner,[15] K. W. Edwards,[15] P. Naik,[15] R. A. Briere,[16] T. Ferguson,[16] G. Tatishvili,[16] H. Vogel,[16] M. E. Watkins,[16] J. L. Rosner,[17] N. E. Adam,[18] J. P. Alexander,[18] K. Berkelman,[18] D. G. Cassel,[18] J. E. Duboscq,[18] R. Ehrlich,[18] L. Fields,[18] R. S. Galik,[18] L. Gibbons,[18] R. Gray,[18] S. W. Gray,[18] D. L. Hartill,[18] B. K. Heltsley,[18] D. Hertz,[18] C. D. Jones,[18] J. Kandaswamy,[18] D. L. Kreinick,[18] V. E. Kuznetsov,[18] H. Mahlke-Krüger,[18] D. Mohapatra,[18] P. U. E. Onyisi,[18] J. R. Patterson,[18] D. Peterson,[18] J. Pivarski,[18] D. Riley,[18] A. Ryd,[18] A. J. Sadoff,[18] H. Schwarthoff,[18] X. Shi,[18] S. Stroiney,[18] W. M. Sun,[18] T. Wilksen,[18] S. B. Athar,[19] R. Patel,[19] V. Potlia,[19] J. Yelton,[19] P. Rubin,[20] C. Cawlfield,[21] B. I. Eisenstein,[21] I. Karliner,[21] D. Kim,[21] N. Lowrey,[21] M. Selen,[21] E. J. White,[21] J. Wiss,[21] R. E. Mitchell,[22] and M. R. Shepherd[22]

(CLEO Collaboration)

[1]*University of Kansas, Lawrence, Kansas 66045*
[2]*Luther College, Decorah, Iowa 52101*
[3]*University of Minnesota, Minneapolis, Minnesota 55455*
[4]*Northwestern University, Evanston, Illinois 60208*
[5]*State University of New York at Albany, Albany, New York 12222*
[6]*State University of New York at Buffalo, Buffalo, New York 14260*
[7]*University of Oklahoma, Norman, Oklahoma 73019*
[8]*University of Pittsburgh, Pittsburgh, Pennsylvania 15260*
[9]*University of Puerto Rico, Mayaguez, Puerto Rico 00681*
[10]*Purdue University, West Lafayette, Indiana 47907*
[11]*Rensselaer Polytechnic Institute, Troy, New York 12180*
[12]*University of Rochester, Rochester, New York 14627*
[13]*Syracuse University, Syracuse, New York 13244*
[14]*Wayne State University, Detroit, Michigan 48202*
[15]*Carleton University, Ottawa, Ontario, Canada K1S 5B6*
[16]*Carnegie Mellon University, Pittsburgh, Pennsylvania 15213*
[17]*Enrico Fermi Institute, University of Chicago, Chicago, Illinois 60637*
[18]*Cornell University, Ithaca, New York 14853*
[19]*University of Florida, Gainesville, Florida 32611*
[20]*George Mason University, Fairfax, Virginia 22030*
[21]*University of Illinois, Urbana-Champaign, Illinois 61801*

[22]*Indiana University, Bloomington, Indiana 47405*

Abstract

Using the CLEO III detector, we measure absolute cross sections for $e^+e^- \to$ hadrons at seven center-of-mass energies between 6.964 and 10.538 GeV. The values of R, the ratio of hadronic and muon pair production cross sections, are determined within 2% total r.m.s. uncertainty.

I. INTRODUCTION

The total cross section for hadron production in electron-positron annihilation is often expressed in terms of the ratio $R(s)$ of the radiation-corrected measured hadronic cross section to the calculated lowest-order cross section for muon pair production. That is,

$$R(s) = \sigma_0(e^+e^- \to \text{hadrons})/\sigma_0(\mathrm{e}^+\mathrm{e}^- \to \mu^+\mu^-), \tag{1}$$

where $\sigma_0(e^+e^- \to \mu^+\mu^-) = 4\pi\alpha^2/3s$. In the simplest form of the quark model $R(s)$ is $R_0(s)$, the sum of the squares of the charges for the quark species allowed by energy conservation, including a factor of $N_c = 3$ for the colors. For energies between $c\bar{c}$ and $b\bar{b}$ thresholds, $R_0 = 3\Sigma_{udsc}Q_f^2 = 10/3$, where Q_f represents the charge of the quark $f = u, d, s, c$.

The strong interactions of the quarks can be accounted for in a perturbation theory expansion in the QCD coupling $\alpha_s(s)$. In the modified minimal-subtraction scheme at the four-loop level [1]:

$$\begin{aligned} R(s) &= R_0 \left[1 + C_1 \frac{\alpha_s(s)}{\pi} + C_2 \left(\frac{\alpha_s(s)}{\pi} \right)^2 \right. \\ &\qquad \left. + C_3 \left(\frac{\alpha_s(s)}{\pi} \right)^3 + O(\alpha_s^4(s)) \right]. \end{aligned} \tag{2}$$

For the four-flavor case the coefficients are $C_1 = 1$, $C_2 = 1.525$, and $C_3 = -11.686$ [1], [2]. Asymptotic freedom in QCD implies that the coupling α_s is not a constant but a smoothly decreasing function of s. The aim of the present experiment is to use measurements of $R(s)$ to make an accurate test of this relation in the 48.5 to 111.0 GeV^2 region of s, where u, d, s, and c quarks are produced.

We use data collected at seven center-of-mass energies at the Cornell Electron Storage Ring (CESR). Electrons and positrons are stored at equal energies in oppositely rotating orbits in the Cornell Electron Storage Ring (CESR), and they collide at a 2 mrad angle at the center of the CLEO III detector [3]. Charged tracks are reconstructed in a 4-layer silicon strip detector and a 47-layer wire drift chamber, and their momenta are determined from their radii of curvature in a 1.5 T magnetic field created by a superconducting solenoid with its axis aligned along the average of the two colliding beam lines. The CsI scintillator shower calorimeter forms a cylindrical barrel around the tracking volume, covering polar angles θ with respect to the beam axis with $|\cos\theta| < 0.85$, supplemented by endcaps extending the range to $|\cos\theta| < 0.93$. Electromagnetic showers are detected with an r.m.s. resolution of about 75 MeV at 5 GeV.

II. ANALYSIS OVERVIEW

To obtain the continuum hadronic annihilation cross section referred to in Eqs. (1, 2), we must correct the observed yield for detection efficiency, for initial state radiation including its influence on efficiency, for other higher order QED effects, and for contributions from the radiative tails of lower energy resonances. We write the observed continuum hadronic cross section as the sum of σ_{sv} from soft photon radiation and virtual higher order diagrams, plus σ_{hard} from hard photon radiation, plus σ_{res} from radiative tails of lower mass $q\bar{q}$ bound states [4–7]:

$$\sigma_{\rm obs}(s) = \sigma_{\rm sv}(s) + \sigma_{\rm hard}(s) + \sigma_{\rm res}(s). \tag{3}$$

The sum of the soft and virtual term can be expressed as

$$\sigma_{\rm sv}(s) = \epsilon(0)\sigma_0(s)\delta_{\rm sv}, \tag{4}$$

where $\epsilon(0)$ is the detection efficiency for events with no initial state radiation, σ_0 is the desired corrected hadronic Born cross section, and $\delta_{\rm sv} = \delta_0 + \delta_{\rm vp}$ accounts for soft photon emission and hadronic and leptonic vacuum polarization:

$$\delta_0 = \frac{2\alpha}{\pi}\left(\frac{3}{4}\ln\frac{s}{m_e^2} + \frac{\pi^2}{6} - 1\right), \tag{5}$$

and

$$\delta_{\rm vp} = \sum_f \frac{2\alpha}{\pi}\left(\frac{1}{3}\ln\frac{s}{m_f^2} - \frac{5}{9}\right), \tag{6}$$

where $f = e, \mu, \tau, h$. A more accurate approximation of hadronic vacuum polarization can be found in reference [8].

The hard photon piece involves an integral of the continuum cross section over all radiated energies [9]:

$$\sigma_{\rm hard}(s) = \sigma_0(s) I_{\rm hard}, \tag{7}$$

with

$$\begin{aligned} I_{\rm hard} \;=\; & \int_0^{k_{\rm max}} \epsilon(k)\left(\frac{\sigma_0^{\rm cont}(s')}{\sigma_0^{\rm cont}(s)}\right) \times \\ & \frac{t}{k^{1-t}}\left(1 - k + \frac{k^2}{2}\right) dk, \end{aligned} \tag{8}$$

where $k = (s - s')/s$ is the normalized radiated energy, $\sqrt{s'}$ is the center of mass energy after the initial state radiation, and the number of equivalent radiation lengths is

$$t = \frac{2\alpha}{\pi}\left(\ln\frac{s}{m_e^2} - 1\right). \tag{9}$$

Before making corrections to the observed continuum hadronic cross section, we first have to subtract the contributions from lower energy $q\bar{q}$ resonances excited through the radiative process $e^+e^- \to \gamma q\bar{q}$ (the last term in Eq. (3)). For each contributing resonance the corresponding term in $\sigma_{\rm res}$ is given by the product of the detection efficiency $\epsilon(k)$, the non-radiative cross section energy integral (given in terms of the resonance coupling Γ_{ee} to e^+e^-, the resonance hadronic branching ratio $B_{\rm had}$, and the resonance mass M), and the radiative kernel, $F(k, s)$:

$$\sigma_{\rm res}(s) = \sum \epsilon(k)\left(\frac{6\pi^2}{M^2}\Gamma_{ee}B_{\rm had}\right) F(k, s), \tag{10}$$

where the sum runs over all known low energy resonances which contributes observed hadronic cross section. In lowest order the kernel can be written as

$$F(k,s) \approx \frac{2M}{s}\frac{t}{k^{1-t}}\left(1 - k + \frac{k^2}{2}\right), \tag{11}$$

with $k = (s - s')/s = 1 - M^2/s$. A higher order representation of $F(k,s)$ can be found in reference [10].

The goal of the measurement, the Born cross section, is derived from Eqs. (3), (4), and (7),

$$\sigma_0(s) = \frac{\sigma_{\rm obs}(s) - \sigma_{\rm res}(s)}{\epsilon(0)\delta_{\rm sv} + I_{\rm hard}}. \tag{12}$$

It is obtained from the observed hadronic cross section, $\sigma_{\rm obs} = (N_{\rm had} - N_{\rm bkg})/(\epsilon_{\rm trigger} \times \int \mathcal{L}dt)$, where $N_{\rm had}$ is the number of detected events passing hadronic event selection criteria, $N_{\rm bkg}$ is the number of background events passing the same requirements, $\epsilon_{\rm trigger}$ is the trigger efficiency correction, and $\int \mathcal{L}dt$ is the integrated luminosity. The background includes e, μ, and τ pairs, virtual photon-photon (two-photon) interactions ($e^+e^- \to e^+e^-\gamma^*\gamma^* \to e^+e^-$ hadrons), beam-gas (beam particle interactions with residual gas molecules) and beam-wall interactions (beam particle interacts with the beam pipe material), and cosmic rays.

III. DATA SAMPLES

The center-of-mass energies $\sqrt{s}$ and integrated luminosities $\int \mathcal{L}dt$ used here are listed in Table I.

TABLE I: Center-of-mass energies and integrated luminosities.

Energy GeV	Luminosity pb^{-1}
10.538	$904.50 \pm 0.30 \pm 9.00$
10.330	$149.80 \pm 0.10 \pm 1.60$
9.996	$432.60 \pm 0.20 \pm 4.80$
9.432	$183.00 \pm 0.10 \pm 2.00$
8.380	$6.78 \pm 0.02 \pm 0.06$
7.380	$8.48 \pm 0.02 \pm 0.07$
6.964	$2.52 \pm 0.01 \pm 0.02$

The luminosities for these data were calculated from measured rates of three different QED processes, $e^+e^- \to e^+e^-$, $\gamma\gamma$, and $\mu^+\mu^-$, using predicted cross sections from the Babayaga MC generator [11], with selection criteria similar to those in Ref. [12]. Particular care was taken to include the effects of $\Upsilon(nS) \to l^+l^-$, where l stands for lepton: e or μ, from either direct production or with an intermediate radiative return [10]. The resulting luminosities from all three reactions were found to be consistent within their systematic uncertainties of 1.8%, 1.2%, and 1.2% for the $\gamma\gamma$, e^+e^-, and $\mu^+\mu^-$ channels, respectively, and a single value at each energy was obtained by combining the three values according to their relative total uncertainties. The total relative uncertainty on the combined luminosity varied from 0.9-1.1%, depending upon energy.

To study efficiencies and backgrounds we used GEANT-based Monte Carlo simulations [13], Jetset 7.3 [14] for hadronic events, and KORALB [15] for τ pairs.

IV. EVENT SELECTION AND DETECTION EFFICIENCIES

The detector trigger used in the measurement of the hadronic event rate is the logical "or" of the following two sets of requirements: 1) at least three axial-projection charged tracks (tracks which are detected in the inner 16 layers of the drift chamber) and at least one low-threshold electromagnetic shower; 2) at least two stereo-projection charged tracks (tracks which are detected in the outer 31 layers of the drift chamber) and either at least two low-threshold showers or at least one medium-threshold shower. The low (medium) trigger threshold for showers is approximately 150 MeV (750 MeV). We evaluate the efficiency by comparing rates (using the hadronic selection criteria described in the next section) with those obtained in special runs with a much looser detection trigger, namely requiring two or more axial-projection charged tracks. Table II shows the resulting trigger efficiency values, $\epsilon_{\rm trigger}$, for the various energy points. The systematic uncertainties are conservatively taken as the deviations from 100% efficiency.

TABLE II: Trigger efficiency correction $\epsilon_{\rm trigger}$, and net hadronic event detection efficiency $\epsilon(0)$ evaluated for the case of zero initial state radiation energy ($k = 0$). The uncertainties are statistical only.

Energy GeV	$\epsilon_{\rm trigger}$ %	$\epsilon(0)$ %
10.538	99.91 ± 0.01	87.43 ± 0.01
10.330	99.91 ± 0.01	87.42 ± 0.03
9.996	99.89 ± 0.01	87.13 ± 0.03
9.432	99.92 ± 0.01	86.05 ± 0.04
8.380	99.88 ± 0.02	84.71 ± 0.10
7.380	99.87 ± 0.02	82.95 ± 0.10
6.964	99.81 ± 0.03	82.07 ± 0.14

In order to suppress backgrounds from events other than $e^+e^- \to$ hadrons, we apply selection requirements (cuts) to individual tracks and showers as well as to entire events. We now describe these cuts and explain how we estimate their efficiency and associated uncertainties.

Table III lists the requirements for accepting individual tracks and showers. We accept all tracks which have χ^2 per degree of freedom (χ^2/NDF) less than 100. Consistency with the beam collision point is enforced by the cut on d_0, the distance of closest approach of the reconstructed track relative to the beam axis, and on z_0, the distance between that point and the average collision point on the beam axis. The hit fraction is the ratio of the number of detected and expected hits when a track passes through the drift chamber, and the θ is

TABLE III: Cuts used to select tracks and showers.

Variable	Allowed range
χ^2/NDF	$<$ 100.0
hit fraction	$(0.5, 1.2)$
$\mid d_0 \mid$	$<$ 3.0 cm
$\mid z_0 \mid$	$<$ 18.0 cm
error of z_0	$<$ 25.0 cm
$\mid \cot(\theta) \mid$	$<$ 3.0424
error of $\cot(\theta)$	$<$ 0.50
$P_{\text{track}}/E_{\text{beam}}$	$(0.01, 1.5)$
$E_{\text{shower}}/E_{\text{beam}}$	> 0.01

the polar angle of the track relative to the beam axis. We require that each track candidate carry at least 1% of the beam momentum. To avoid poorly measured tracks, we require that the ratio of the track momentum to the beam momentum be less than 1.5. We require that each accepted shower carry at least 1% of the beam energy and that no track be associated with it.

The event selection criteria are listed in Table IV, and their description are provided in the following paragraphs.

TABLE IV: Hadronic event selection criteria.

Variable	Allowed range
$\mid Z_{\text{vertex}} \mid$	< 6.0 cm
$E_{\text{vis}}/(2E_{\text{beam}})$	> 0.5
$\mid P_{\text{z}}^{\text{miss}}/E_{\text{vis}} \mid$	< 0.3
H_2/H_0	< 0.9
$E_{\text{cal}}/(2E_{\text{beam}})$	$(0.15, 0.9)$
$E_\gamma^{\text{max}}/E_{\text{beam}}$	< 0.8
$N_{\text{ChargedTrack}}$	≥ 4

The event Z_{vertex} is the weighted average of the z_0's of the charged tracks, and weights are defined as $1/\sigma_{z_0}^2$, where σ_{z_0} is the uncertainty of the z_0. The purpose of this cut was to suppress background due to beam-gas, beam-wall collisions and from cosmic rays. The measured R value was sensitive at the level of only 0.16% to the cut over the range from 4 to 10 cm.

The visible energy E_{vis} is defined as the sum of charged particle energies computed from the track momenta assuming pion masses, plus the neutral shower energies measured in the electromagnetic calorimeter. We normalize the visible energy to the center-of-mass energy so that we can use the same cut for all runs. The visible energy cut is designed to suppress background from virtual photon-photon collisions and from beam-gas interactions. Figure 1 shows the normalized visible energy distribution at 9.996 GeV. We varied the cut in scaled

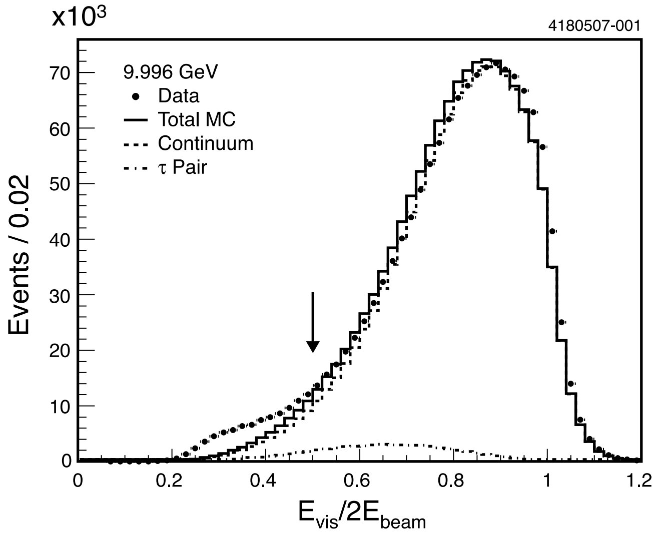

FIG. 1: Visible energy distribution at 9.996 GeV, normalized to center-of-mass energy, when all cuts are applied except the one shown. In this as well as in all other figures, arrows indicate cut values.

visible energy ($E_{\rm vis}/(2E_{\rm beam})$) from its nominal level of 0.5 down to 0.3 and to 0.4 to estimate our sensitivity to the two-photon background. We also varied the cut upwards to 0.6 and to 0.7 to estimate the discrepancy between data and Monte Carlo.

The background from two-photon and beam-gas events was also suppressed by the cut on the ratio $\mid P_z^{\rm miss}/E_{\rm vis} \mid$ of the z-component of the event missing momentum and visible energy (see Fig. 2). The R results varied by less than 0.65% over the cut range 0.2 to 0.4.

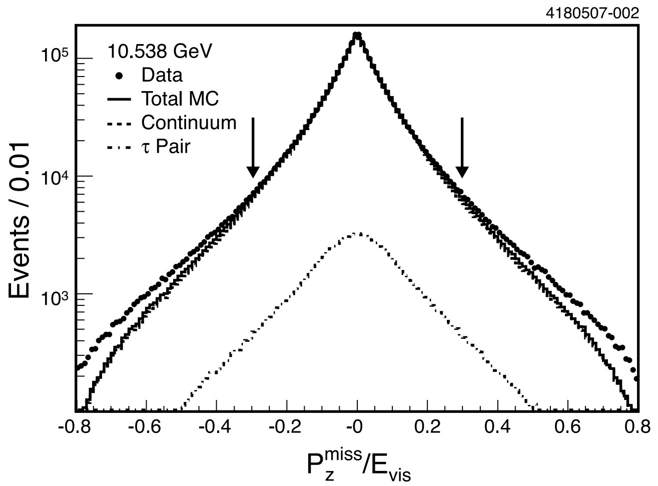

FIG. 2: The ratio of the z-component of the event missing momentum to event visible energy $P_z^{\rm miss}/E_{\rm vis}$ at 10.538 GeV.

The typical signature of a QED event (e, μ, or τ pair) is low charged track multiplicity which would fail the four-track requirement, although higher multiplicity decays of taus are likely to pass. We rely on calorimeter information to suppress the remaining background further. The distribution of the ratio of calorimeter energy $E_{\rm cal}$, which includes isolated showers as well as track matched showers, to the center-of-mass energy, is plotted in Fig. 3. It shows a contribution at low values from tau-pairs and, at $E_{\rm cal}/(2E_{\rm beam}) = 1$, a contribution from Bhabha-scattered electron pairs. The cuts eliminated both extremes. Varying the upper cut from 0.8 to ∞ made less than 0.49% difference in R values.

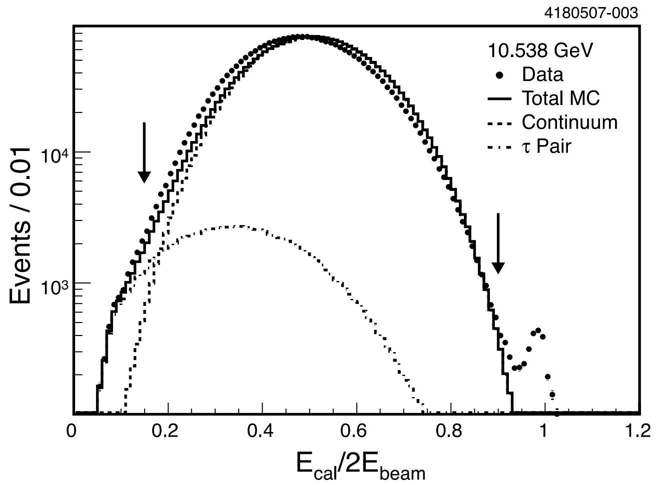

FIG. 3: The ratio of calorimeter energy of charged and neutral particles to $2E_{\rm beam}$ at 10.538 GeV.

Figure 4 shows the distribution of the ratio of Fox-Wolfram moments H_2/H_0 [16]. The QED process $e^+e^- \to l^+l^-$, where $l = e, \mu$ or τ, results in a high value of this ratio. Cut variation above 0.8 produced a variation in R of less than 0.54%.

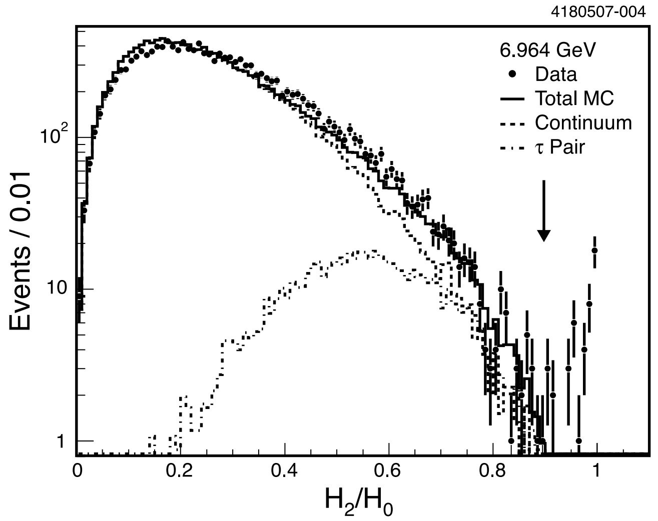

FIG. 4: Distribution of the ratio of Fox-Wolfram moments H_2/H_0 at 6.964 GeV.

We also studied the ratio of the energy of the most energetic unmatched shower to the beam energy, shown in Fig. 5. To suppress production of hadronic events at low center-of-mass energies through initial state radiation, we cut at 0.80. Varying the cut from 0.6 to infinity changed the value of R less than 0.40%.

The charged track multiplicity cut also suppressed QED events in our hadronic sample. The multiplicity distribution (see Fig. 6) showed a significant sensitivity of the accepted

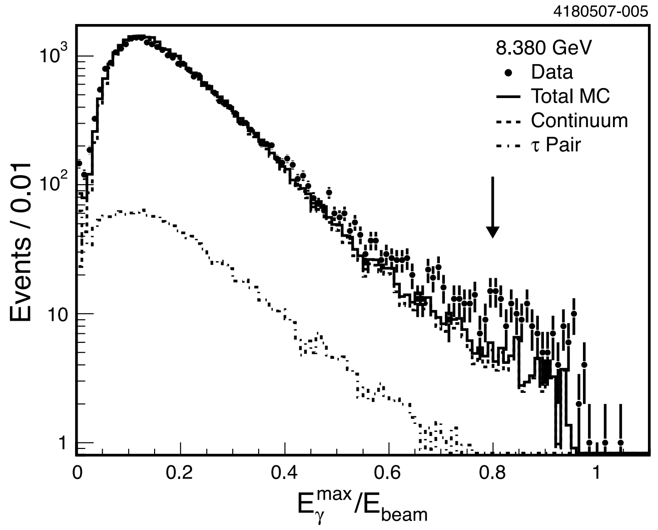

FIG. 5: The ratio of the most energetic shower energy to the beam energy at 8.380 GeV.

rate to the chosen cut level. However, there is a discrepancy between data and the Monte Carlo simulation. The discrepancy at lower multiplicity values can be explained by the contribution of QED events; the discrepancy at higher multiplicity values can be explained by inaccuracies at the Monte Carlo generator level.

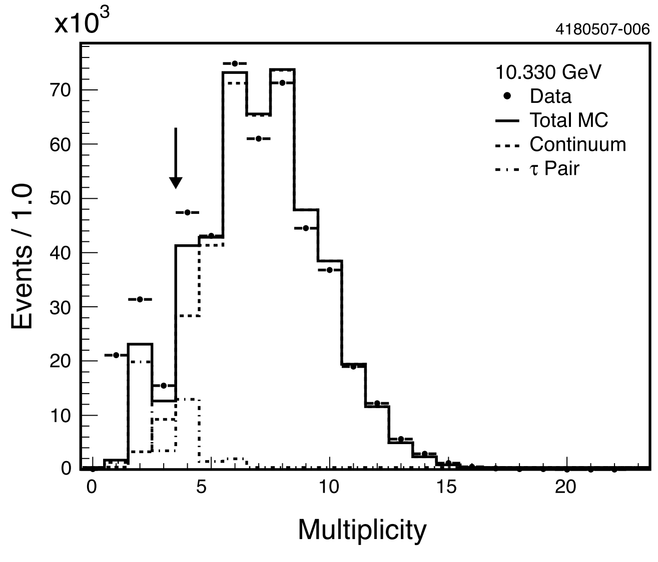

FIG. 6: Charged particle multiplicity distribution at 10.330 GeV.

The selection criteria defined in Tables III and IV were used to determine the number of hadronic events and the hadronic detection efficiencies for the various incident beam energies, using our data and Monte Carlo samples (see Tables II and V). We performed the efficiency calculation using weights assigned to each continuum multiplicity value instead of relying on the continuum Monte Carlo prediction for the multiplicity distribution. The weights were assigned by comparing data multiplicity with continuum and τ-pair Monte

Carlo samples:

$$w_n = \frac{N_n^{\rm data} - N_n^{\tau-{\rm pair}}}{N_n^{\rm cont}}, \tag{13}$$

where w_n is the weight which is assigned to a continuum event with multiplicity n; $N_n^{\rm data}$, $N_n^{\tau-{\rm pair}}$, and $N_n^{\rm cont}$ are the number of events in the data sample, τ-pair, and continuum Monte Carlo samples with multiplicity n, respectively. Since low multiplicity values are contaminated by e^+e^- and $\mu^+\mu^-$ events, we assign a weight of 1.0 for multiplicities less than three.

Figure 7 shows the k-spectra, relative decrease in squared center-of-mass energy due to initial state radiation, The step near $k = 0.84$ represents the $c\bar{c}$ threshold. Table II summarizes the no-radiation hadronic event detection efficiencies $\epsilon(0)$, and Fig. 8 shows how the hadronic event detection efficiency varies with k.

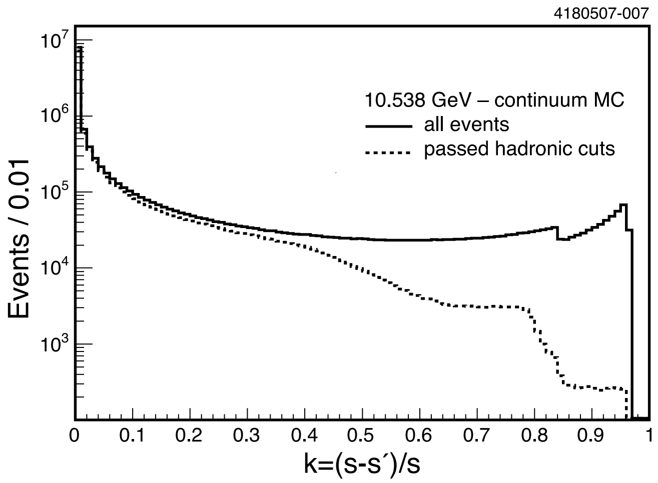

FIG. 7: k distribution of the Monte Carlo continuum sample at 10.538 GeV.

V. BACKGROUND

Sources of background were suppressed with the help of our hadronic event selection criteria. We deal with the remaining level of background events from two-photon, beam-gas, and beam-wall interactions, as well as from τ-pair, μ-pair, and Bhabha production in the following. Figure 9 shows the net charge distribution of hadronic events that pass the hadronic event selection criteria. The Monte Carlo (continuum + τ-pair) describes our data well, however, there are small discrepancies in the tails (Figs. 1-6). These discrepancies may be related to the beam-gas or beam-wall interactions not included in our Monte Carlo samples. We estimated and subtracted the number of τ-pair events using the known QED cross section and the KORALB [15] Monte Carlo simulation.

The two-photon interactions, which are the dominant source of background after τ-pairs, were studied with a dedicated Monte Carlo that generated $e^+e^- \to e^+e^- +$ hadrons events. We found that the portion of two-photon events which survive our selection criteria with a loose cut $E_{\rm vis}/2E_{\rm beam} \geq 0.2$ (our nominal cut is 0.5) changes from 1.52% at 10.538 GeV to

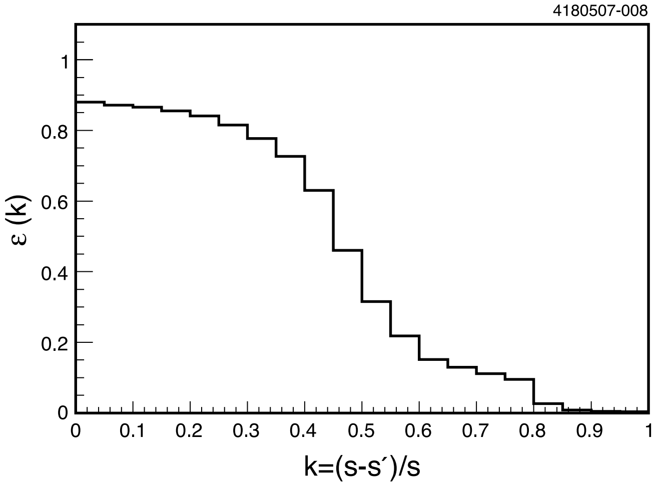

FIG. 8: Hadronic event detection efficiency as a function of k at 9.996 GeV.

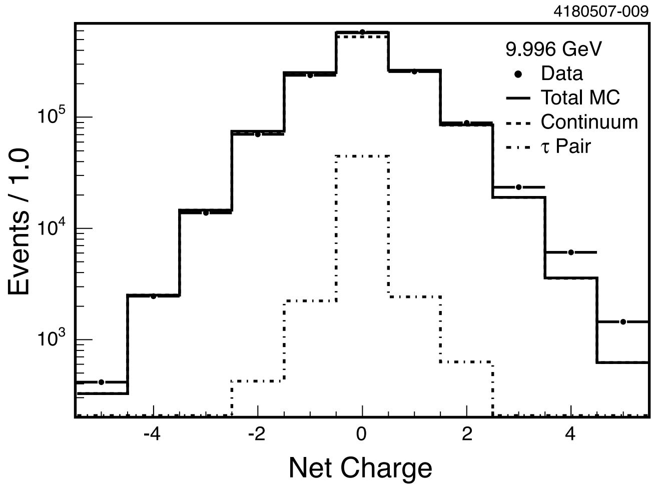

FIG. 9: Net charge distribution of events at 9.996 GeV.

0.5% at 6.964 GeV. For this reason, instead of subtracting the two-photon background, we have varied the $E_{\rm vis}/2E_{\rm beam}$ cut to assign an additional contribution to the event selection systematic uncertainty in R.

VI. RESONANCE EFFECTS AND RADIATIVE CORRECTION

The beams radiate energy before the annihilation interaction and can then create $c\bar{c}$ and $b\bar{b}$ bound state resonances. When the resonance decays to hadrons, our observed cross section increases. For the purposes of our R measurement, these contributions are sources of background and must be subtracted. The following resonances were considered: Υ(3S), Υ(2S), Υ(1S), ψ(4160), ψ(3770), ψ(2S), and J/ψ. To take into account the resonance contributions we use Eqs. (10) and (3). For this purpose we used the CLEO-measured dielectron widths of Υ(1S), Υ(2S), and Υ(3S) from Ref. [18] and dielectron widths of J/ψ and ψ(2S) from Ref. [19]. We used dielectron widths of ψ(3770) and ψ(4160) from the

PDG [20]. Table V shows the total cross section of contributing resonances and the ratio of the resonance contribution to the observed cross section for each energy point. We used a sample of low-background charged dipion transition events in data to check our calculated quarkonium contributions to our observed hadronic sample. Selecting $\Upsilon(3S)$, $\Upsilon(2S)$, and $\psi(2S)$ resonance production through initial state radiation from 10.538 GeV, we studied the following transitions: $\Upsilon(3S) \to \pi^+\pi^-\Upsilon(1S)$, $\Upsilon(2S) \to \pi^+\pi^-\Upsilon(1S)$, and $\psi(2S) \to \pi^+\pi^- J/\psi$, where $\Upsilon(2S)$, $\Upsilon(1S)$, and J/ψ decay to $\mu^+\mu^-$, to estimate resonance contributions at our highest-luminosity point, 10.538 GeV. We found that our experimental results agreed with the theoretical expectation for these modes within 1.5 standard deviations.

TABLE V: Number of hadronic events after background subtraction, radiation and efficiency corrections, total and relative contribution of resonances through radiative return, and interference effect.

Energy GeV	Hadronic events	$\epsilon(0)\delta_{\rm sv} + I_{\rm hard}$	$\sigma_{\rm res}$ nb	$\sigma_{\rm res}/\sigma_{\rm obs}$ %	Interfer-ence %
10.538	2426337	0.935	0.056	2.08	-
10.330	403743	0.935	0.044	1.62	0.14
9.996	1988179	0.931	0.033	1.14	0.22
9.432	573516	0.919	0.001	0.03	0.51
8.380	26705	0.901	0.003	0.09	-
7.380	42204	0.879	0.009	0.14	-
6.964	14508	0.867	0.009	0.17	-

Since three runs were at energies just below the Upsilon resonance masses, interference between the continuum and the resonance can affect the measured continuum cross section. The magnitude and sign of this effect depends on the difference between the center-of-mass energy and the resonance mass. The CESR beam energy spread, which is of order 4 MeV, convolves the interference effects from different center-of-mass energies, yielding an overall negative effect on the measured cross section below resonance. In the last column of Table V are listed calculated corrections to the continuum cross section to compensate upward for the effect of interference and beam energy spread [18].

We applied the procedure described in Section II by evaluating the $\epsilon(0)\delta_{\rm sv} + I_{\rm hard}$ term of Eq. (12) to calculate the radiative correction for each incident energy point. The efficiencies at different values of k (see Fig. 8) from continuum Monte Carlo have been used to calculate $I_{\rm hard}$. Table V shows the radiation and efficiency factor [see Eq. (12)] corrections for each energy. The decrease of $\epsilon(0)\delta_{\rm sv} + I_{\rm hard}$ with energy mainly comes from the efficiency decrease (see Table II).

VII. SYSTEMATIC UNCERTAINTIES AND RESULTS

The following have been considered as sources of systematic uncertainty for each continuum cross section measurement: luminosity, radiative correction, trigger efficiency for hadronic events, multiplicity correction, and hadronic event selection criteria (see Table VI).

The hadronic vacuum polarization terms in Eq. (6) are of the order of 0.01. Since they dominate the uncertainty in the radiative correction, we have assigned a 1% uncertainty in σ_0 from this source.

Each selection criterion, except for multiplicity, has independently been varied by about 20% to estimate its systematic uncertainty. Moreover, we used a visible energy $E_{\text{vis}}/2E_{\text{beam}}$ cut variation of about 40% to assign an additional systematic uncertainty related to the two-photon background and the visible energy shift: we assign half the difference between R values obtained with cuts on $E_{\text{vis}}/2E_{\text{beam}}$ of 0.3 and 0.4 (0.6 and 0.7) as systematic uncertainty associated with two-photon background (visible energy shift).

Even though the multiplicity cut was part of the hadronic event selection criteria, we assigned a separate systematic uncertainty to our correction procedure by taking the difference between the corrected and uncorrected R values at the nominal cut level. The summary of all systematic uncertainties is given in Table VI. At each energy we divide the systematic uncertainty into a common uncertainty that correlated across all energy points and an uncorrelated uncertainty that is independent for each energy point. The decrease of the uncorrelated systematic uncertainty with decreasing beam energy is mainly due to the energy dependence of the two-photon interaction background cross section.

TABLE VI: Systematic uncertainty (in %) assigned to each energy point. The last two rows show common and uncorrelated uncertainties.

Energy (GeV)	10.538	10.330	9.996	9.432	8.380	7.380	6.964
Luminosity	1.00	1.10	1.10	1.10	0.90	0.90	1.00
Trigger	0.09	0.09	0.11	0.08	0.12	0.13	0.19
Radiative correction	1.00	1.00	1.00	1.00	1.00	1.00	1.00
Multiplicity correction	1.06	1.38	0.99	0.84	0.43	0.38	0.38
Hadron event selection	1.51	1.09	1.31	1.31	1.05	1.02	0.79
Total	2.32	2.30	2.21	2.15	1.76	1.74	1.68
Common	1.87	1.67	1.85	1.87	1.62	1.64	1.58
Uncorrelated	1.37	1.59	1.22	1.05	0.70	0.57	0.55

Values of R for each of the energy points are shown in Table VII and are presented in Fig. 10 along with MARK I [21], MD1 [22], Crystal Ball [23], and prior CLEO [17] results. Our new measurements of R are in good agreement with previous MD1, Crystal Ball, and CLEO measurements; however, they do not agree with the MARK I results.

Table VIII shows the α_s values obtained by solving Eq. (2) (with four flavors) for α_s at each of the seven energies (extraction of α_s when quark masses are taken into account can be found in reference [24]). Comparing α_s values with the QCD predictions [25] at our energies, which assumes the combined world average of $\alpha_s(M_Z^2) = 0.1189 \pm 0.0010$, we find agreement within our quoted uncertainties. Moreover, we compare our results at 10.330, 9.996, and 9.432 GeV energies with CLEO measurements [26] at Υ(1S), Υ(2S), and Υ(3S) energies, which are based on direct photon spectrum studies, and we find a good agreement within our quoted uncertainties as well.

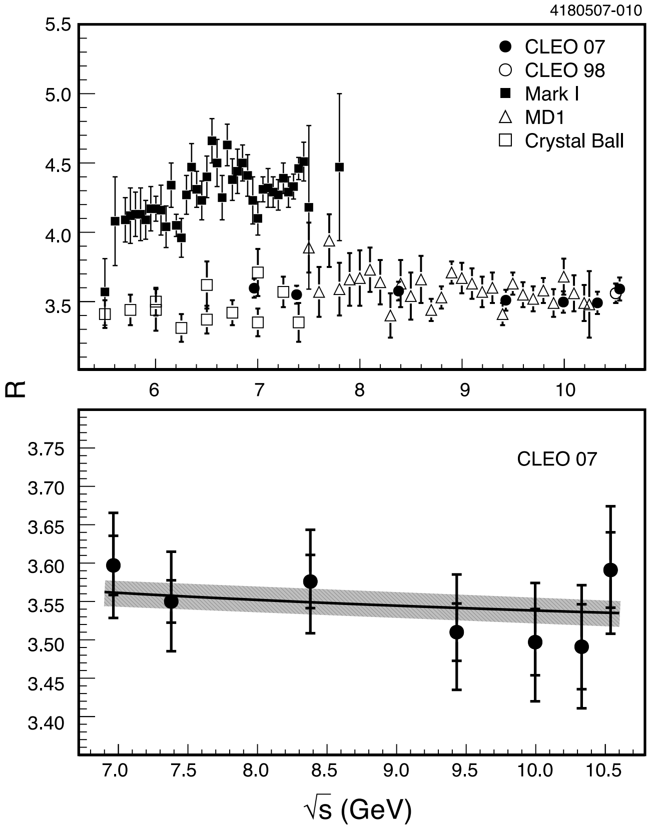

FIG. 10: R measurement at 5.0 - 10.5 GeV c.m. energies. The top figure compares our measurement with other experiments [20]. The bottom plot shows our new results,where two sets of uncertainties represent combined uncorrelated and statistical uncertainties and total uncertainties; the line represents Eq. (2) with our average $\Lambda = 0.31$ GeV, and the shaded area indicates the R-values corresponding to one standard deviation in the uncorrelated systematic uncertainty in Λ.

TABLE VII: Measured values of $R(s)$ with statistical and systematic (common and uncorrelated) uncertainties, respectively.

$\sqrt{s}$ GeV	$R(s)$
10.538	$3.591 \pm 0.003 \pm 0.067 \pm 0.049$
10.330	$3.491 \pm 0.006 \pm 0.058 \pm 0.055$
9.996	$3.497 \pm 0.004 \pm 0.064 \pm 0.043$
9.432	$3.510 \pm 0.005 \pm 0.066 \pm 0.037$
8.380	$3.576 \pm 0.024 \pm 0.058 \pm 0.025$
7.380	$3.550 \pm 0.019 \pm 0.058 \pm 0.020$
6.964	$3.597 \pm 0.033 \pm 0.057 \pm 0.020$

TABLE VIII: Derived values of $\alpha_s(s)$ with statistical and systematic (common and uncorrelated) uncertainties, respectively using the prescription outlined in the text.

$\sqrt{s}$ GeV	$\alpha_s(s)$
10.538	$0.232 \pm 0.003 \pm 0.061 \pm 0.045$
10.330	$0.142 \pm 0.005 \pm 0.051 \pm 0.049$
9.996	$0.147 \pm 0.004 \pm 0.057 \pm 0.038$
9.432	$0.159 \pm 0.004 \pm 0.058 \pm 0.033$
8.380	$0.218 \pm 0.022 \pm 0.053 \pm 0.023$
7.380	$0.195 \pm 0.017 \pm 0.052 \pm 0.018$
6.964	$0.237 \pm 0.030 \pm 0.052 \pm 0.018$

To test the compatibility with other measurements of α_s we note the expected running of α_s with energy [20]:

$$\begin{aligned}\alpha_s(s) \; = \; & \frac{4\pi}{\beta_0 \ln(s/\Lambda^2)} \left[1 - \frac{2\beta_1}{\beta_0^2} \frac{\ln[\ln(s/\Lambda^2)]}{\ln(s/\Lambda^2)} \right. \\ & + \frac{4\beta_1^2}{\beta_0^4 \ln^2(s/\Lambda^2)} \times \left(\left(\ln\left[\ln(s/\Lambda^2)\right] - \frac{1}{2} \right)^2 \right. \\ & \left. \left. + \frac{\beta_2 \beta_0}{8\beta_1^2} - \frac{5}{4} \right) \right], \end{aligned} \tag{14}$$

where n_f presents the number of quarks which have mass less than $\sqrt{s}/2$, Λ represents the QCD energy scale, and the β-functions are defined as follows: $\beta_0 = 11 - 2n_f/3$, $\beta_1 = 51 - 19n_f/3$, and $\beta_2 = 2857 - 5033n_f/9 + 325n_f^2/27$.

To find Λ, we use our α_s values at each energy point and solve Eq. (14), assuming n_f is equal to 4. The value of Λ varies from 0.11 at 10.330 GeV to 0.67 at 10.538 GeV. Using Eq. (14) with our average value of Λ, we extract the value of the α_s at $\sqrt{s} = M_Z$. Our results for α_s imply $\Lambda = 0.31^{+0.09+0.29}_{-0.08-0.21}$ GeV and $\alpha_s(M_Z^2) = 0.126 \pm 0.005 \; ^{+0.015}_{-0.011}$, where the uncertainties represent statistical and total systematic, respectively.

Our results for $\alpha_s(M_Z^2)$ and $\Lambda(n_f = 4)$ agree with the world averages $\alpha_s(M_Z^2) = 0.1189 \pm 0.0010$ [25] and $\Lambda(n_f = 4) = 0.29 \pm 0.04$ GeV [27].

In conclusion, we have shown that our measurements of $R(s)$ are consistent with the QCD predictions of Eq. (1) and Eq. (14) with better precision than previous measurements of $R(s)$. However, since the Eq. (1) dependence of $R(s)$ on $\alpha_s(s)$ is only in higher order terms, we do not have a determination of $\alpha_s(s)$ or Λ that is competitive with measurements by other methods.

We gratefully acknowledge the effort of the CESR staff in providing us with excellent luminosity and running conditions. D. Cronin-Hennessy and A. Ryd thank the A.P. Sloan Foundation. This work was supported by the National Science Foundation, the U.S. Department of Energy, and the Natural Sciences and Engineering Research Council of Canada.

---

[1] L.R. Surguladze and M.A. Samuel, Phys. Rev. Lett. **66**, 560 (1991); S.G. Gorishny, A.L. Kataev, S.A. Larin, Phys. Lett. B **259**, 144 (1991).
[2] M Davier and A. Höcker, Phys. Lett. B **419**, 419 (1998).
[3] G. Viehhauser *et al.* (CLEO Collaboration), Nucl. Instrum. Methods Phys. Res., Sect. A **462**, 146 (2001).
[4] F.A. Berends and R. Kleiss, Nucl. Phys. B **178**, 141 (1981).
[5] G. Bonneau and F. Martin, Nucl. Phys. B **27**, 381 (1971).
[6] J. Schwinger, Phys. Rev. **76**, 760 (1949); F.A. Berends and G.J. Komen, Phys. Lett. **63**, 432 (1976).
[7] A. Osterheld *et al.*, SLAC-PUB-4160 (1986).
[8] H. Burkhardt and B. Pietrzyk, Phys. Rev. D **72**, 057501 (2005); H. Burkhardt and B. Pietrzyk, Phys. Lett. B **356**, 398 (1995).
[9] Bonneau and Martin [5] divide the radiated energy spectrum between $\sigma_{\rm sv}$ and $\sigma_{\rm hard}$ at $k_0 \ll 1$. For convenience, Behrends and Kleiss [4] (and we) remove $1 - t\ln k_0$ from σ_0 and add it to $\sigma_{\rm hard}$ by extending the hard integral down to $k = 0$.
[10] E.A. Kuraev and V.S. Fadin, Sov. J. Nucl. Phys. **41**, 466 (1985).
[11] C.M. Carloni Calame *et al.*, Nucl. Phys. Proc. Suppl. **131**, 48 (2004); C.M. Carloni Calame, Phys. Lett. B **520**, 16 (2001); C.M. Carloni Calame *et al.*, Nucl. Phys. B **584**, 459 (2000).
[12] G. Crawford *et al.* (CLEO Collaboration), Nucl. Instrum. Methods Phys. Res., Sect. A **345**, 429 (1994).
[13] R. Brun *et al.*, GEANT 3.21, CERN Programming Long Writeup Report No. W5013, 1993 (unpublished).
[14] T. Sjöstrand, Computer Physics Commun. **82**, 74 (1994).
[15] S. Jadach and Z. Wąs, Comp. Phys. Commun. **85**, 453 (1995).
[16] G.C. Fox and S. Wolfram, Phys. Rev. Lett. **41**, 1581 (1978); G.C. Fox and S. Wolfram, Nucl. Phys. B **149**, 413 (1979); G.C. Fox and S. Wolfram, Phys. Lett. B **82**, 134 (1979).
[17] R. Ammar *et al.* (CLEO Collaboration), Phys. Rev. D **57**, 1350 (1998).
[18] J.L. Rosner *et al.* (CLEO Collaboration), Phys. Rev. Lett. **96**, 092003 (2006).
[19] G.S. Adams *et al.* (CLEO Collaboration), Phys. Rev. D **73**, 051103(R) (2006); N.E. Adam *et al.* (CLEO Collaboration), Phys. Rev. Lett. **96**, 082004 (2006).
[20] S. Eidelman *et al.* (Particle Data Group), Phys. Lett. B **592**, 1 (2004).
[21] J.L. Siegrist *et al.*, Phys. Rev. D **26**, 969 (1982).
[22] A.E. Blinov *et al.*, Z. Phys. C **49**, 239 (1991); A.E. Blinov *et al.*, Z. Phys. C **70**, 31 (1996).
[23] Z. Jakubowski *et al.*, Z. Phys. C **40**, 49 (1988); C. Edwards *et al.*, SLAC-PUB-5160 (1990).
[24] J.H. Kühn, M. Steinhauser and T. Teubner, arXiv:0707.2589.
[25] S. Bethke, Prog. Part. Nucl. Phys. **58**, 351 (2007).
[26] D. Besson *et al.* (CLEO Collaboration), Phys. Rev. D **74**, 012003 (2006).
[27] S. Bethke, Nucl. Phys. Proc. Suppl. **135**, 345 (2004).